RSC Advances

PAPER

View Article Online
View Journal | View Issue

Cite this: *RSC Adv.*, 2017, **7**, 23272

Effect of pyrazolium-derived compounds as templates in zeolite synthesis

Peicheng Wang,[a] Yang Zhao,[a] Hongbin Zhang,*[a] Tao Yu,[b] Yahong Zhang[a] and Yi Tang*[a]

A series of diquaternary pyrazolium-derived organic templates (*N*,*N*′-dimethyl-*N*,*N*′-1,6-dihexylidenedipyrazolium, *N*,*N*′-diethyl-*N*,*N*′-1,6-dihexylidenedipyrazolium, *N*,*N*′-dipropyl-*N*,*N*′-1,6-dihexylidenedipyrazolium, denoted as 6C-DMP, 6C-DEP, 6C-DPP, respectively) with methyl, ethyl and propyl groups substituted on the N atom of pyrazole ring at both terminals have been used in the synthesis of high silica MTW and MFI zeolites. Through combining the characterization results, including XRD, NMR, elemental analysis, TG, XRF, FE-SEM, N_2 sorption and FE-TEM, with molecular mechanics simulations to explore the location, orientation and the interaction energies of the three templates, we confirmed the state of templates in zeolite framework, carefully characterized their morphology/structure properties, and finally investigated their different spatial effects for the zeolite formation. The study found that 6C-DMP and 6C-DEP are able to produce MTW, while 6C-DPP is able to produce MFI. 6C-DMP, owing to a good match with the MTW framework and can be used to synthesize regular MTW zeolite with few defects. The MTW zeolite prepared by using 6C-DEP as a template presents more defects and irregular macromorphology due to a relatively poor match to the MTW framework. 6C-DPP can get MFI other than MTW due to a larger spatial hindrance, and it is located in the MFI framework with a special spatial orientation.

Received 9th March 2017
Accepted 21st April 2017

DOI: 10.1039/c7ra02864d

rsc.li/rsc-advances

1. Introduction

Zeolites are crystalline porous materials with regular and uniform microporous channel structures. Until now, there are more than 200 kinds of zeolites with varied framework topologies in which the size, shape, dimension and orientation of micropores, and even the composition and corresponding acid/alkali/redox characters can be selectively regulated.[1–3] With the pore diameter in molecular scale (0.3–1.3 nm), the selective separation and absorption of various guest molecules can be achieved based on the distinct size and shape of zeolite micropores.[4,5] Additionally, owing to the high surface area, favourable hydrothermal stability, and good mechanical properties, zeolites have been widely used as solid catalysts in current chemistry industry.[6–8]

Zeolites are usually synthesized under hydrothermal conditions, and the synthesis system is rather complicated with the addition of Si/Al species, mineralizer, inorganic species and organic compounds.[9–11] Quaternary ammonium is the mostly used organic compounds which is also called templates. In 1961, Barrer and Denny introduced tetramethyl ammonium cation (TMA^+) into the synthesis system of zeolite A for the first time.[12] Since then, extensive research has been focusing on the effect of organic templates (*e.g.* quaternary ammoniums) in zeolite synthesis, and meanwhile a series of zeolites with diverse frameworks were synthesized.[13–15] Despite these remarkable achievements, the role of organic templates and their host–guest interaction has not yet been clearly expounded.[16–19]

Recently, much progress has been made to design distinctive organic templates, among which diquaternary ammonium is a kind of important templates with good flexibility and feasibility.[20–26] Its end groups and chain length can be selectively altered to facilitate the formation of diverse microporous topology, and even sometimes to tailor the crystal morphology or mesoporosity. Thereinto, Moini *et al.* investigated the directing role of $(CH_3)_3N^+(CH_2)_nN^+(CH_3)_3$ by regulating $(CH_2)_n$ length, in which they found that EUO zeolite can be produced with $n = 5$, 6, NEI zeolite with $n = 10$, MTT zeolite with $n = 7$, 8, 9, 11, 12, and MTW with $n = 9$, 14.[20] Thus, the chain length n plays a key role in the resulting zeolite phase, and only specific chain length can provide an ideal fit for the formation of certain zeolites. Similarly, Camblor *et al.*[15] used the diquaternary templates of two quinuclidinium heads linked by a chain of 4, 6 or 8 CH_2 groups to synthesize silica zeolites. The study found that zeolites Beta, MFI, MTW, ITQ-8, IYQ-10, and ITQ-14 could

[a]*Department of Chemistry, Laboratory of Advanced Materials, Collaborative Innovation Center of Chemistry for Energy Materials, Shanghai Key Laboratory of Molecular Catalysis and Innovative Materials, Fudan University, Shanghai 200433, People's Republic of China. E-mail: yitang@fudan.edu.cn; zhanghongbin@fudan.edu.cn*

[b]*Department of Chemistry, College of Arts and Sciences, Tennessee Technological University, Cookeville, TN 38505-0001, USA*

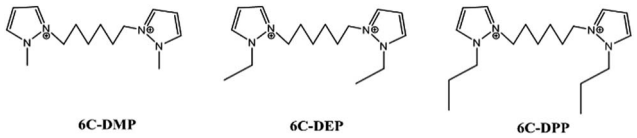

Scheme 1 Templates used in this work.

be prepared with varied CH_2 chain lengths under different synthesis conditions. These researches all verified that the important role of $(CH_2)_n$ chain length of diquaternary ammonium.[21–23] However, besides the length in the axis direction, the spatial effect of its head also matters in the synthesis of zeolite.[24–26]

In order to explore the spatial effects of long CH_2 templates on its radical direction, we designed three pyrazolium-derived compounds with 1,6-hexylidene as linker, and pyrazole ring is substituted by methyl, ethyl or propyl (denoted as 6C-DMP, 6C-DEP and 6C-DPP, respectively Scheme 1). Each alkyl group stretches along the radical direction and is perpendicular to the long CH_2 chain in space. These three organic compounds are used as templates to produce a series of zeolite samples under various hydrothermal conditions. Their distinctive structure directing effect has been systematically investigated by combination of zeolite structures/morphologies characterization and molecular mechanics simulations.

2. Experiments

2.1 Materials

1-Methyl-pyrazole (Accela ChemBio Co., Ltd., 98%), 1-ethyl-pyrazole (Accela ChemBio Co., Ltd., 98%), 1-propal-pyrazole (Accela ChemBio Co., Ltd., 95%) and 1,6-dibromolhexane (Aladdin Industrial Co., 97%) were used as raw reagents for the preparation of pyrazolium-derived organic compounds. Acetonitrile (Sinopharm Chemical Reagent Co. Ltd, AR) was used as solvent. Acetone (Sinopharm Chemical Reagent Co. Ltd, AR) was used to wash away residual reagents and purify the organic compounds.

For the preparation of zeolite samples, aluminum chloride hexahydrate ($AlCl_3 \cdot 6H_2O$, Sinopharm Chemical Reagent Co. Ltd, AR) was used as aluminum source, and sodium hydroxide (NaOH, Sinopharm Chemical Reagent Co. Ltd, AR) was used to get the alkaline solution. Colloidal silica (LUDOX HS-40, 40 wt%, aqueous solution) was used as silica source. Deionized water was used as solvent.

2.2 Synthesis of organic templates

The three organic compounds consisted of doubly charged quaternary cations were synthesized by reaction of 1,6-dibromohexane with the corresponding pyrazole derivatives according to the ref. 22 and 27. In a typical synthesis of 6C-DMP, 16.42 g of 1-methylpyrazole was dissolved in 30 ml of acetonitrile. 11.6 g of 1,6-dibromohexane was add to the solution, which was then kept under magnetic stirring at 90 °C for 4 days. The solution was cooled and the bromide ammonium salt was separated by filtration, followed by washing with a large amount of acetone. The product was obtained by rotatory evaporation. As for 6C-DEP and 6C-DPP, a similar procedure was taken to obtain the compounds. The purity of the ammonium salts was confirmed by liquid ^{13}C NMR on Bruker AVANCE III HD spectrograph.

2.3 Synthesis of zeolite samples

Zeolite samples were prepared in hydrothermal synthesis. The composition of the synthesis system is xNaOH : $0.02AlCl_3 \cdot 6H_2O$: 0.16R : SiO_2 : yH_2O where $x = 0.15$–0.25; $y = 20$–40; R = 6C-DMP; 6C-DEP; 6C-DPP. In a typical synthesis, 0.107 g of $AlCl_3 \cdot 6H_2O$ was dissolved in 14 g of deionized water, and 1.512 g of 6C-DMP was added as template. After stirring for 30 min, 0.222 g of sodium hydroxide was added to the mixture and 3.33 g of aqueous colloid silica was added until the sodium hydroxide dissolved completely. After stirring and agitation for 3 h, the clear mixture solution was transferred into a Teflon-lined autoclave which was heated at 160 °C for 2–4 days. The resulted solid samples were isolated by filtration and washing with deionized water for several times followed by drying at 80 °C.

2.4 Characterization of zeolite samples

The zeolite samples were identified by powder X-ray diffraction (XRD) on a Bruker D8-Advanced diffractometer using Cu Kα radiation between 5 and 50° (2θ values) at 40 kV and 40 mA. Morphology of the zeolite samples was observed by FE-SEM on Hitachi S-4800. Crystal defects of the zeolite samples were observed by FE-TEM on JEM-2100F. Characterization of sample structure were obtained by solid NMR spectrum (^{29}Si and ^{13}C MAS NMR) on Bruker 400WB AVANCE III spectrograph. CHN element analysis for identifying the organic compounds was conducted on Analysensysteme GmbH vario EL Elemental Analyzer. X-ray fluorescence (XRF) was conducted on Bruker S4EXPLORER. TG curves were obtained on TA SDT-Q600, with a heating rate of 10 °C min^{-1} from 25 to 950 °C. The zeolite samples were calcined at 550 °C for 6 h in air to remove templates. After calcination, low temperature N_2-sorption were conducted on Quantachrome autosorb iQ-2 instrument at 77 K.

2.5 Computational methods

According to ref. 28 computational methodology was used based on molecular mechanics simulations to study the structure directing effect of the three pyrazolium-derived compound for zeolite-framework formation. The simulations were carried out through the Forcite Module in Materials Studio.[29] The structure of MTW and MFI zeolite were obtained from the website of International Zeolite Association. In all the calculations, the geometry of the zeolite framework was fixed and the periodic boundary conditions (PBC) were applied. The CVFF forcefield[23] was employed to obtain the interaction energies between the templates and the zeolite framework. DFT calculations were conducted to obtain the atomic charges of the pyrazolium templates by using B3LYP hybrid functional associated with 6-31++g(d,p) basis sets and the ESP method.[30] Uniform charge background method[31] was used for zeolite

framework to balance the positive charge of pyrazolium templates. The charges of framework oxygen were fixed to −0.3, and the charge of framework silicon atom was calculated to keep total charge neutrality.

By using Monte-Carlo simulations, through the Sorption Module in Material Studio,[28] the diquaternary pyrazolium templates were docked in the zeolite framework. The most stable structure and location of the templates were obtained by using simulated annealing search in the Forcite Module. Through subtracting the energy of the molecules in vacuum to the total energy of the system, the interaction energies were figured out. The interaction energy values are given in unit of kcal per mol per unit cell.

3. Results and discussion

3.1 Synthesis modulation and product phase region

The zeolite synthesis results (using three pyrazolium-derived organic templates) are shown in Table 1. All these pyrazolium templates can direct the zeolite formation, but they show a different selection for the zeolite phase. For 6C-DMP, under low H_2O/Si ratio condition only amorphous phase could be obtained. When the H_2O/Si ratio is raised to 30, MTW zeolite can be produced after a 2 days of crystallization. Prolonging crystallization time to 4 days or increasing the H_2O/Si ratio to 40, MTW zeolite can still be obtained. For 6C-DEP, the synthesis results are similar to 6C-DMP. Under low H_2O/Si ratio (H_2O/Si = 20), no crystalline product is observed even after a 7-days crystallization, while MTW zeolite could be obtained when H_2O/Si ratio is higher than 30. For 6C-DPP, special cases are found under similar synthesis conditions. Crystalline product cannot be obtained in low H_2O/Si ratio (H_2O/Si = 20), but when H_2O/Si ratio was raised to 30, MFI zeolite could be produced. And MFI zeolite could still be obtained when H_2O/Si ratio was raised to 40 with the crystallization time prolonged to 7 days. Noticed that MTW cannot be obtained by using 6C-DPP. In summary, when the alkyl groups substituted on N atoms at the terminal of pyrazolium are methyl or ethyl groups, MTW zeolite can be prepared, but when it turns to propyl group, it does not contribute to the MTW synthesis, but it can facilitate the formation of MFI.

Table 1 Synthesis conditions and product phases

SDA	H_2O/Si	OH^-/Si	Time/days	Phase
6C-DMP	20	0.25	4	Amorphous
	30	0.25	2	MTW
	30	0.25	4	MTW
	40	0.25	4	MTW
6C-DEP	20	0.25	7	Amorphous
	30	0.25	4	MTW
	30	0.50	4	MTW
	40	0.25	4	MTW
6C-DPP	20	0.15	7	Amorphous
	20	0.20	4	Amorphous
	30	0.25	4	MFI
	40	0.25	4	MFI
	40	0.25	7	MFI

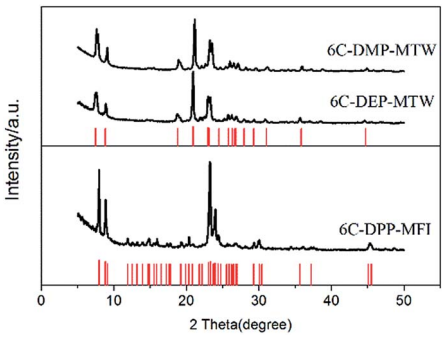

Fig. 1 XRD pattens of 6C-DMP-MTW, 6C-DEP-MTW, 6C-DPP-MFI. The red line represents the characteristic diffraction of zeolite MTW and MFI (from http://www.iza-online.org/).

Here, in order to study the relations between templates and the structure/morphology properties of zeolite products, three typical samples were selected from Table 1, which are all synthesised at fixed H_2O/Si ratio (40) and crystallization time (4 days) with addition of 6C-DMP, 6C-DEP or 6C-DPP.

The XRD patterns (Fig. 1) show that they are all pure zeolite phase with high crystallinity. The former two samples display the typical pattern of zeolite MTW while the latter can be easily be identified as zeolite MFI. No any peak belonging to impurity phase was observed in the pattern of the three samples. We named them by "template name-zeolite phase", *i.e.* 6C-DMP-MTW, 6C-DEP-MTW, 6C-DPP-MFI, respectively.

3.2 Characterization of the state of templates in framework

The state of templates in framework were conducted through a series of characterizations. The liquid ^{13}C NMR of the three organic compounds exhibit high degree of structural integrity and purity (Fig. 2, red line). All the peaks have been marked and could be assigned to different C atoms of the templates. To determine whether the templates were decomposed during the hydrothermal process, the corresponding solid state ^{13}C MAS NMR of the three zeolite samples were detected as shown in Fig. 2.

Each peak in ^{13}C MAS NMR spectra (black line) could match well with that in the liquid ^{13}C NMR spectra of corresponding templates. This indicates that the three templates are all introduced into the zeolite framework and remain relatively intact with nearly no decomposition under hydrothermal conditions.

For further determining the existing form of the three templates, the CHN analysis was employed to detect the precise C/N ratio of templates in zeolite samples as shown in Table 2. The corresponding results (C/N = 3.6, 4.1 and 4.6) are very close to the theoretical value of these three templates (C/N = 3.5, 4.0 and 4.5), implying that no decomposition of pyrazolium templates occured and they intactly participated in zeolite crystallization.

In order to obtain the composition of the three samples, we detected the mass of templates in framework by TG experiment. The weight loss for templates are about 9.45, 11.12 and 12.47% for 6C-DMP-MTW, 6C-DEP-MTW, and 6C-DPP-MFI, respectively. Taking into consideration of the real Si/Al ratios as shown in Table 2, we successfully calculated the exact composition formula

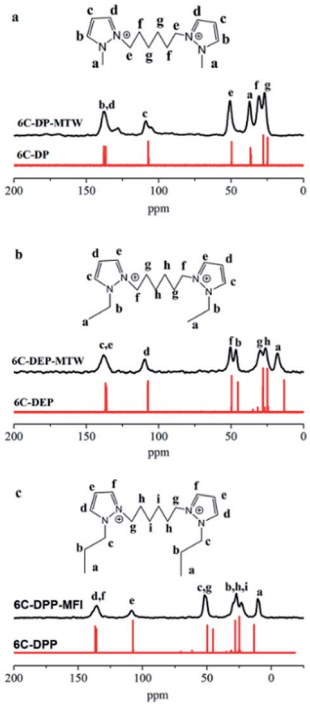

Fig. 2 Liquid ^{13}C NMR spectrum (red line) of (a) 6C-DMP, (b) 6C-DEP, (c) 6C-DPP and solid-state ^{13}C MAS NMR spectrum (black line) of (a) 6C-DMP-MTW, (b) 6C-DEP, (c) 6C-DPP-MFI.

(seeing Table 2), which indicates that about one template molecule is incorporated within per MTW unit cell for 6C-DMP-MTW and 6C-DEP-MTW, but about two 6C-DPP molecules incorporated within per MFI unit cell for 6C-DPP-MFI.

3.3 Characterization on morphology/structure properties

The three templates lead to different synthesis results (Table 1 and Fig. 1), and the minute differences between the three zeolite samples are detected to investigate the directing role of these templates. FE-SEM is employed to characterize the macro- and mesomorphology of the three samples (Fig. 3). Both 6C-DMP and 6C-DEP can direct the formation of MTW, but the morphology of the two as-made MTW zeolite samples are significantly different. 6C-DMP-MTW (Fig. 3a and b) shows a nanorod-stacking and shuttle-like regular morphology with a relatively smooth external surface. Despite the similar shuttle-like shape (Fig. 3c and d), 6C-DEP-MTW exhibits an apparent nanoparticle-assembled fine structure, and some smaller-sized

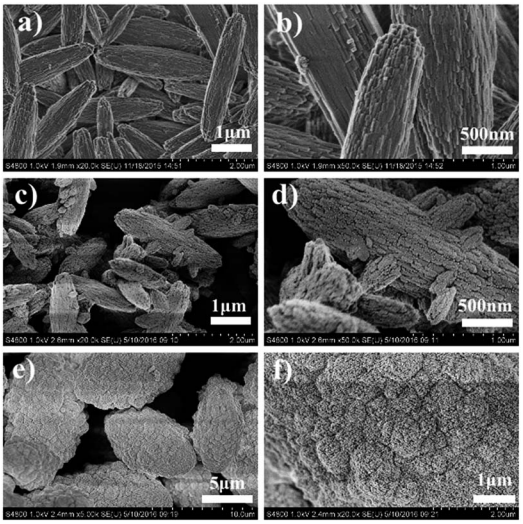

Fig. 3 FE-SEM image of (a, b) 6C-DMP-MTW, (c, d) 6C-DEP-MTW, (e, f) 6C-DPP-MFI.

branching crystals have been observed on its rough surface. Interestingly, compared with 6C-DEP-MTW, 6C-DPP-MFI, although it is quite another phase, also shows a nanocrystallite-assembled structure but with an axiolitic shape (Fig. 3e and f). This nanoparticle-assembled morphology may indicate that there was a poorly crystal growth during the hydrothermal process.

In consideration of the different macromorphology of the three zeolite samples, N_2-sorption experiments are adopted to characterize their micro/mesoporous properties. The three samples all show I–IV type isotherm but with subtle distinctions (Fig. 4). In detail, the steep increases at $P/P_0 < 0.1$ are similar for 6C-DMP-MTW and 6C-DEP-MTW (Fig. 4a and b) due to their same microporous properties and similar crystallinity, while 6C-DPP-MFI (Fig. 4c) shows a higher step here because of the more open two-dimensional micropore structure. Moreover, for the intermediate and high relative pressure, the isotherms of 6C-DEP-MTW and 6C-DPP-MFI (Fig. 4b and c) are more similar with an enhanced adsorption at $0.2 < P/P_0 < 1$ but without the characteristic stepping down around $P/P_0 = 0.43$ in desorption branch. This phenomenon should arise from nitrogen adsorption on the open inter-crystallite mesopores formed by assembly of adjacent nano-crystallites, in agreement with the SEM images in Fig. 3d and f. Table 3 shows the detailed textural data. The microporous volume of 6C-DMP-MTW is close to that

Table 2 Chemical composition of the three zeolites samples

Samples	% C[a]	% N[a]	C/N[b]	Si/Al[c]	Formula[d]
6C-DMP-MTW	3.8	1.2	3.6 (3.5)	43	$[6C\text{-}DMPBr_2]_{0.9}[Si_{54.7}Al_{1.3}O_{112}]$
6C-DEP-MTW	4.8	1.4	4.1 (4)	40	$[6C\text{-}DEPBr_2]_{1.0}[Si_{54.6}Al_{1.4}O_{112}]$
6C-DPP-MFI	5.7	1.5	4.6 (4.5)	41	$[6C\text{-}DPPBr_2]_{1.8}[Si_{93.7}Al_{2.3}O_{192}]$

[a] Mass percent given by CHN analyst. [b] Molar ratio. The theoretical value is given in parentheses. [c] Si/Al is given by XRF. [d] Formula is given by TG analyst.

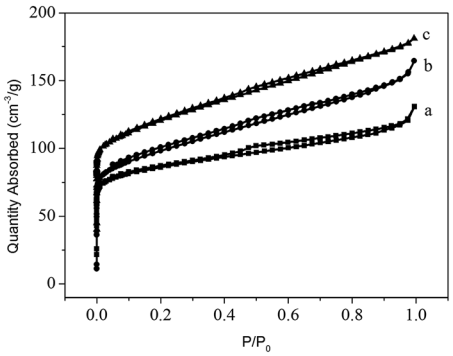

Fig. 4 Nitrogen sorption isotherms for (a) 6C-DP-MTW, (b) 6C-DEP-MTW, and (c) 6C-DPP-MFI.

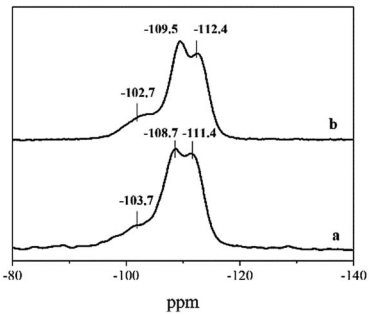

Fig. 5 ^{29}Si MAS NMR spectrum of (a) 6C-DMP-MTW, (b) 6C-DEP-MTW.

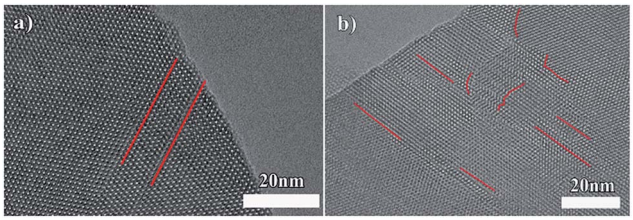

Fig. 6 FE-TEM images of (a) 6C-DMP-MTW; (b) 6C-DEP-MTW. Defects are marked with red lines.

of 6C-DEP-MTW, while the latter has a larger external surface and mesoporous volume. Despite the large microporous volume, the 6C-DPP-MFI shows similar external surface area and mesoporous volumes with 6C-DEP-MTW.

6C-DMP-MTW and 6C-DEP-MTW are of the same zeolite phase, but their morphology and textural properties are quite different. This unique phenomenon was further investigated by using ^{29}Si MAS NMR and FE-TEM, which reveal the microstructure properties of the two samples. ^{29}Si MAS NMR spectrum of 6C-DMP-MTW (Fig. 5a) shows two peaks at −108.7 and −111.4 ppm, corresponding to Si (0Al). The two peaks are assigned to Si atoms in different tetrahedral sites in the MTW framework.[32,33] The signal with chemical shift at −102.7 ppm corresponds to either Si (1Al) or SiOH groups. For 6C-DEP-MTW spectrum (Fig. 5b), there are two chemical shifts at −109.5 and −112.4 ppm, corresponding to Si (0A1) in different tetrahedral sites in the framework. And the chemical shift at −103.7 ppm can be attributed to Si (1Al) or SiOH groups. An increase of the relative intensity of the signal at −103 ppm was caused probably by the increase of SiOH groups which probably refers to a relatively large amount of defects in 6C-DEP-MTW.[32] FE-TEM was further employed to characterize the defects of microstructure in 6C-DMP-MTW and 6C-DEP-MTW.[34,35] 6C-DMP-MTW exhibits a high degree of structural integrity and only a few defects are observed (red line, Fig. 6a). But there were a large amount of defects in 6C-DEP-MTW (Fig. 6b), which exhibits a low degree of structural integrity. The clear and distinct defects correspond well to the differences in morphology and textural properties, *i.e.* the differences in macroscopic property is probably caused by the crystal mesostructure. Compared with 6C-DMP-MTW, a large number of structure defects in 6C-DEP-MTW caused the poor crystal growth and irregularly crystal morphology. And all these differences might derive from the different construction of the two templates 6C-DMP and 6C-DEP.

Above experiment results indicate the applying of different templates with different terminals will give rise to varieties in macro-, meso- and micro-morphology/structure, and even defects in 6C-DMP-MTW, 6C-DEP-MTW. Therefore the distinctive directing role of diquaternary pyrazolium are further studied through fitness of these templates in the zeolite framework.

3.4 Computational simulations

In order to analyze the different behaviors of the three diquaternary pyrazolium templates in the zeolite formation at a molecular level, we applied molecular mechanics simulations to understand the structure directing roles by exploring the position and orientation of the three templates in the zeolite channels, as well as their interaction energies with the zeolite framework. The numbers of template molecules included in the zeolite framework were obtained from the sample formula given in Table 2. Firstly, for 6C-DMP-MTW system, we used Monte-Carlo simulations followed by simulated annealing search to

Table 3 Textural properties of 6C-DMP-MTW, 6C-DEP-MTW and 6C-DPP-MTW

Samples	S_{BET}[a] ($m^2 \cdot g^{-1}$)	S_{ext}[b] ($m^2 \cdot g^{-1}$)	V_{micro}[b] ($cm^3 \cdot g^{-1}$)	V_{total}[c] ($cm^3 \cdot g^{-1}$)	V_{meso}[d] ($cm^3 \cdot g^{-1}$)
6C-DMP-MTW	325	67	0.11	0.20	0.09
6C-DEP-MTW	357	128	0.10	0.26	0.16
6C-DPP-MFI	441	144	0.13	0.28	0.15

[a] By BET method. [b] By *t*-plot method. [c] Evaluated at $p/p_0 = 0.99$. [d] $V_{meso} = V_{total} - V_{micro}$.

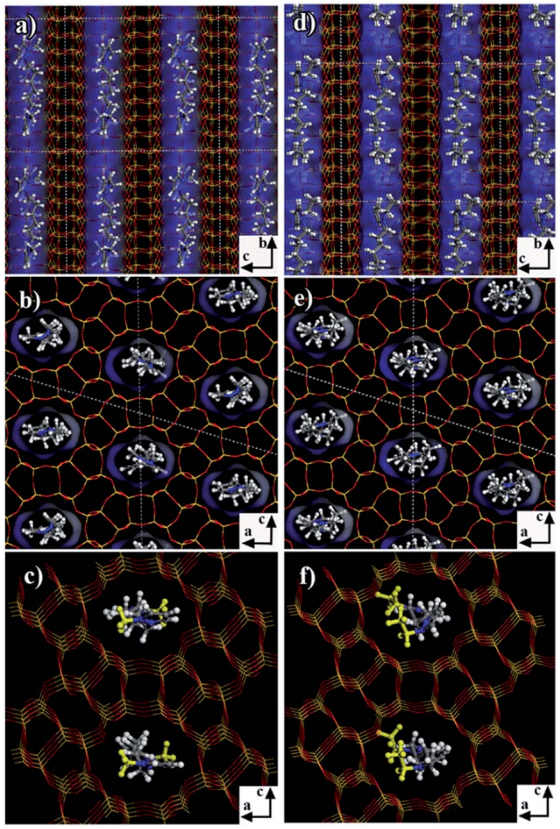

Fig. 7 Snapshot of (a–c) the 6C-DMP located in the MTW channel, (d–f) the 6C-DEP located in the MTW channel. The channel was highlighted by blue. The methyl and ethyl groups are highlighted by yellow in (e) and (f).

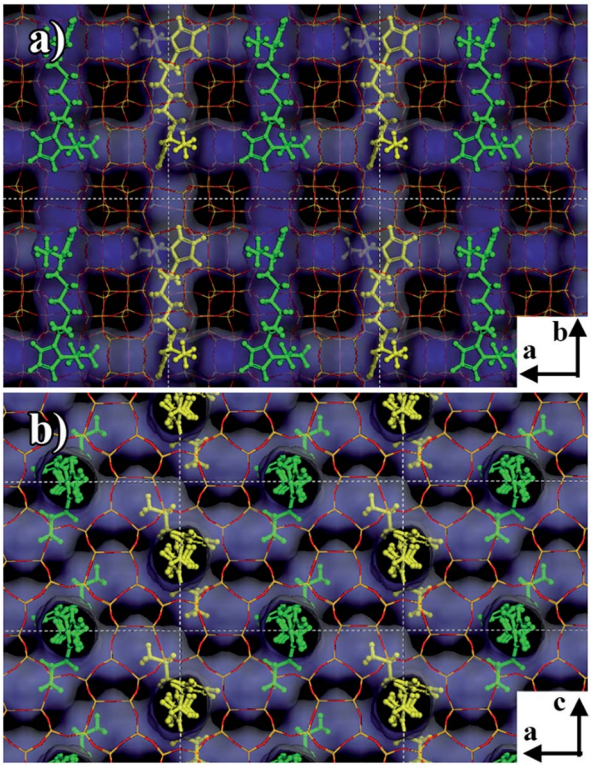

Fig. 8 Snapshot of the 6C-DPP located in the MFI zeolite channel. The channel was highlighted by blue. The yellow and green are shown to differentiate two types of molecular locations.

study how 6C-DMP incorporated into the MTW zeolite channels, and obtain the most stable structure of the 6C-DMP molecules embedded in the channels. Displayed in Fig. 7a–c, the 6C-DMP is located orderly in the 12-member ring straight channel of the MTW along with the *b* axis, and methyl groups are in the opposite side of CH_2 chain (Fig. 7c). The interaction energy is −596.8 kcal per mol per unit cell. In addition, it is found that the 6C-DEP molecule is also located in the straight channel of the MTW, and it is oriented along the *b* axis with ethyl groups being in the same side of CH_2 chain, shown in Fig. 7d–f. The calculated interaction energy is −580.6 kcal per mol per unit cell. Comparing the 6C-DMP with 6C-DEP, we found that the former has slightly larger interaction energy, indicating that the 6C-DMP can fit into the MTW channel better than the other. Such an observation can be attributed to the fact that, the smaller methyl group in the 6C-DMP reduced the steric hindrance between the template and framework. Therefore, it is no surprise that the 6C-DEP ethyl group must be located in the same side of the CH_2 chain and twisted in order to fit into the MTW channel and, shown in Fig. 7d–f.

For the 6C-DPP template, the size of 1-propyl-pyrazolium at the terminal of 6C-DPP is 6.94 Å, and the pore dimension of the 12-member ring in *b* axis of MTW is 5.6 × 6.0 Å. Due to the rigid construction of 1-propyl-pyrazolium head, it cannot be distorted, thus cannot be filled into the MTW channel. As a result, the template 6C-DPP cannot be used to produce the MTW zeolite. Then we docked 6C-DPP into the MFI framework, and obtain the most stable 6C-DPP configuration in the channels. As shown in Fig. 8, it is found that 6C-DPP is mainly distributed in the straight channels of the 10-member ring along with the *b* axis of MFI zeolite. In particular the orientation of long CH_2 chain of 6C-DPP is aligned with the *b* axis of MFI. The propyl groups at the two terminals of pyrazolium ring were stretched into two adjacent paralleling sinusoidal channels (along the *a* axis) with one up and the other down. There are two spatial orientations of 6C-DPP (the yellow and green part in Fig. 8). The special position and spatial orientation of 6C-DPP in MFI framework resulted from the periodically appearing of the wave crest and trough in the sinusoidal channels along the *a* axis in the MFI framework. Propyl group on the pyrazolium ring cannot be occluded in the straight channel for the large rigid steric hindrance. As a result, the 6C-DPP has to be twisted so that the propyl group can be stretched into the sinusoidal channel. Secondly, since the length of 1,6-dihexylidene (8.4 Å) of 6C-DPP is well-matched with the length of the adjacent channel intersection (9.5 Å) in the MFI framework. The driving forces stabilizing the 6C-DPP in the MFI-channel is from electrostatics and van der Waals interactions, and the interaction energy of 6C-DPP (2 per unit cell) is −365.1 kcal per mol per unit cell.

With a combination of the experiment results and the molecular mechanics simulations, it is found that the match degree

between templates and zeolite framework, which stemmed from the spatial effect in radial direction, can exert a great influence on the macromorphology of the crystals. Due to the relatively poor match between 6C-DEP and MTW framework with a weaker interaction and a twisted template conformer (Fig. 7), compared with 6C-DMP, the crystal growth is imperfect and a large number of defects were generated. As a result, the high-density dislocation was observed from FE-TEM (Fig. 6) in the 6C-DEP-MTW which further leads to a large number of mesopores (Table 3) and an irregular macromorphology (Fig. 3c and d). In spite of the preference of MFI framework for 6C-DPP template, the similar situation is observed in 6C-DPP-MFI. That is, the match between 6C-DPP and MFI framework is not very well which resulted in a rough surface and nano-crystallite assembled structure.

4. Conclusions

Three diquaternary pyrazolium-derived compound with different spatial size in the radial direction were used as templates in zeolite synthesis. The spatial effect of the templates would affect the zeolite phase selection and would have an effect on the macromorphology of the zeolite. Molecular mechanics simulations show that 6C-DMP has less steric hindrance and it is best matched with the MTW framework, leading to a relatively larger interaction energy and promotion of producing MTW zeolite with regular morphology and less defects. The 6C-DEP can produce MTW with a large amount of defects and a rough macromorphology due to the large bulk of ethyl group. As for 6C-DPP, due to the existence of propyls on the terminals of the pyrazolium, it cannot direct the formation of MTW but can produce MFI with the existence of 6C-DPP in its channels in a special spatial orientation.

Acknowledgements

This work is supported by National Key Basic Research Program of China (2013CB934101), NSFC (21433002, 21573046, and 21473037), China Postdoctoral Science Foundation (2015M580289).

Notes and references

1 M. E. Davis, *Chem. Mater.*, 2014, **26**, 239–245.
2 A. F. Masters and T. Maschmeyer, *Microporous Mesoporous Mater.*, 2011, **142**, 423–438.
3 D. P. Serrano, J. M. Escola and P. Pizarro, *Chem. Soc. Rev.*, 2013, **42**, 4004–4035.
4 A. Corma, *J. Catal.*, 2003, **216**, 298–312.
5 D. Verboekend and J. Pérez-Ramírez, *Catal. Sci. Technol.*, 2011, **1**, 879.
6 K. Na, C. Jo, J. Kim, K. Cho, J. Jung, Y. Seo, R. J. Messinger, B. F. Chmelka and R. Ryoo, *Science*, 2011, **333**, 328–332.
7 H. Zhang, Y. Ma, K. Song, Y. Zhang and Y. Tang, *J. Catal.*, 2013, **302**, 115–125.
8 H. Zhang, Z. Hu, L. Huang, H. Zhang, K. Song, L. Wang, Z. Shi, J. Ma, Y. Zhuang, W. Shen, Y. Zhang, H. Xu and Y. Tang, *ACS Catal.*, 2015, **5**, 2548–2558.
9 C. S. Cundy and P. A. Cox, *Chem. Rev.*, 2003, **103**, 663–702.
10 C. S. Cundy and P. A. Cox, *Microporous Mesoporous Mater.*, 2005, **82**, 1–78.
11 H. Zhang, Y. Zhao, H. Zhang, P. Wang, Z. Shi, J. Mao, Y. Zhang and Y. Tang, *Chem.–Eur. J.*, 2016, **22**, 7141–7151.
12 M. Moliner, F. Rey and A. Corma, *Angew. Chem., Int. Ed.*, 2013, **52**, 13880–13889.
13 D. W. Lewis, D. J. Willock, C. R. A. Catlow, J. M. Thomas and G. J. Hutchings, *Nature*, 1996, **382**, 604–606.
14 P. Wagner, Y. Nakagawa, G. S. Lee, M. E. Davis, S. Elomari, R. C. Medrud and S. I. Zones, *J. Am. Chem. Soc.*, 2000, **122**, 263–273.
15 M. J. Díaz-Cabañas, M. A. Camblor, Z. Liu, T. Ohsuna and O. Terasaki, *J. Mater. Chem.*, 2002, **12**, 249–257.
16 P. Sun, Q. Jin, L. Wang, B. Li and D. Ding, *J. Porous Mater.*, 2003, **10**, 145–150.
17 M. M. Kurmach, P. S. Yaremov, V. V. Tsyrina, M. O. Skoryk and O. V. Shvets, *Theor. Exp. Chem.*, 2015, **51**, 216–223.
18 R. H. Archer, S. I. Zones and M. E. Davis, *Microporous Mesoporous Mater.*, 2010, **130**, 255–265.
19 T. Ikuno, W. Chaikittisilp, Z. Liu, T. Iida, Y. Yanaba, T. Yoshikawa, S. Kohara, T. Wakihara and T. Okubo, *J. Am. Chem. Soc.*, 2015, **137**, 14533–14544.
20 A. Moini, K. D. Schmitt, E. W. Valyocsik and R. F. Polomski, *Zeolites*, 1994, **14**, 504–511.
21 A. Jackowski, S. I. Zones, S. J. Hwang and A. W. Burton, *J. Am. Chem. Soc.*, 2009, **131**, 1092–1100.
22 T. Mandai, M. Imanari and K. Nishikawa, *Chem. Phys. Lett.*, 2012, **543**, 72–75.
23 A. Rojas, L. Gomez-Hortiguela and M. A. Camblor, *J. Am. Chem. Soc.*, 2012, **134**, 3845–3856.
24 A. Rojas and M. A. Camblor, *Dalton Trans.*, 2014, **43**, 10760–10766.
25 R. Kore and R. Srivastava, *RSC Adv.*, 2012, **2**, 10072.
26 O. V. Shvets, N. Kasian, A. t. Zukal, J. i. Pinkas and J. i. Čejka, *Chem. Mater.*, 2010, **22**, 3482–3495.
27 T. V. Goncharova, L. V. Zatonskaya and A. S. Potapov, *Procedia Chem.*, 2014, **10**, 485–489.
28 Y. M. Variani, A. Rojas, L. Gómez-Hortigüela and S. B. C. Pergher, *New J. Chem.*, 2016, **40**, 7968–7977.
29 Forcite Module, Material Studio 7.0, Accelrys Inc.
30 A. K. Rappe and W. A. Goddard, *J. Phys. Chem.*, 1991, **95**, 3358–3363.
31 A. De Vita, M. J. Gillan, J. S. Lin, M. C. Payne, I. Štich and L. J. Clarke, *Phys. Rev. B: Condens. Matter Mater. Phys.*, 1992, **46**, 12964–12973.
32 N. Masoumifard, S. Kaliaguine and F. Kleitz, *Microporous Mesoporous Mater.*, 2016, **227**, 258–271.
33 B. Gil, Ł. Mokrzycki, B. Sulikowski, Z. Olejniczak and S. Walas, *Catal. Today*, 2010, **152**, 24–32.
34 Z. Qin, G. Melinte, J.-P. Gilson, M. Jaber, K. Bozhilov, P. Boullay, S. Mintova, O. Ersen and V. Valtchev, *Angew. Chem., Int. Ed.*, 2016, **55**, 15049–15052.
35 S. Huang, P. Chen, B. Yan, S. Wang, Y. Shen and X. Ma, *Ind. Eng. Chem. Res.*, 2013, **52**, 6349–6356.

